Supplementary Information for: "Non-zero Yarkovsky acceleration for near-Earth asteroid (99942) Apophis"

Jorge A. Pérez-Hernández[1] & Luis Benet[1]

[1] *Instituto de Ciencias Físicas, Universidad Nacional Autónoma de México*

Av. Universidad s/n, Col. Chamilpa, CP 62210 Cuernavaca, Mor., México

Supplementary Note 1: Planetary ephemerides and comparison with DE430

We have implemented our own planetary, lunar and main-belt orbital ephemerides integrator[1]. The dynamical model is based on the formulation of JPL's DE430 ephemeris[2], and involves the Sun, the planets, the Moon, Pluto and the 343 most massive main-belt asteroids. It includes post-Newtonian gravitational interactions for all bodies, except for the main-belt asteroids, whose computation considers only one iteration. We also include the acceleration due to the Sun's J_2 zonal harmonic with all other bodies, the interaction of the Earth zonal harmonics J_2 through J_5 with the Sun, Mercury, Venus, Mars, Jupiter, and the Moon, and the interaction of the Moon zonal and tesseral harmonics up to sixth order with the Sun, Mercury, Venus, Earth, Mars and, Jupiter. The model also includes the long-term change of the Earth's orientation, based on the IAU 1976/1980 precession and nutation models[2–4], considering the 18.6 yr period terms in the lunar mean longitude of the ascending node[3]. The orientation of the Moon is computed numerically from the differential equations for the Euler angles, which are related to the angular velocity of the mantle expressed in the Moon fixed (principal axis) frame. This imposes the computation of several torques upon the Moon; we consider the torques due to the Sun, Mercury, Venus, Mars, Earth and Jupiter[2], torques due to the interaction of the figure of the Moon with the figure of the Earth[2]. The latter computation corresponds to a system of coupled delay differential equations[5]. Finally, the model also includes the secular acceleration upon the Moon due to tides raised on the Earth by the Sun and the Moon using a time-lag model[2,6]. We set the initial conditions for the Sun, the planets, the Moon and, Pluto at the J2000.0 epoch, i.e., January 1st, 2000 12:00 TDB.

In the Supplementary Figure 1 we present the (absolute) differences obtained from our planetary ephemeris integration and DE430 in a 100 yr integration for several Solar System objects. The equations of motion for the Sun, the planets, the Moon, Pluto and the 343 most massive main-belt asteroids are solved using a 25-order Taylor integration scheme, with an absolute tolerance of 10^{-20}. At each time step, the Taylor series (in time) of the position and velocity vectors of each body are stored, and are later used for the integration of the orbit of Apophis.

Supplementary Note 2: Apophis dynamical model

The numerical integration of Apophis orbital motion includes post-Newtonian accelerations due to the Sun, eight planets, the Moon and, Pluto, Newtonian accelerations from the 16 main-belt asteroids listed in the Supplementary Table 1, and the Yarkovsky effect. For Apophis, we set initial conditions using the JPL's #197 solution[7], at the epoch December 17, 2020 00:00:00.0 (TDB). A comparison of different perturbing acceleration magnitudes on Apophis as a function of time shows that the Yarkovsky acceleration is comparable to the gravitational perturbation from Pluto, Pallas and Hygiea, which supports the inclusion of Pluto in the set of perturbing bodies, whenever the perturbations on Apophis from at least the 4 most-massive main-belt asteroids are taken into account[1].

Supplementary Note 3: Numerical methods

The differential equations describing the orbital motion of Apophis described in Section are integrated using the Taylor method[8]. We add the equation $\dot{A}_2 = 0$ as a supplementary differential equation for Apophis. This turns the orbital propagation of Apophis into a 7-DOF problem, and allows us to use the parameter A_2 as an additional initial (unknown) parameter which is constant throughout the integration. Since the time steps are not constant, the integration method has an adaptative step size.

In order to evaluate the high-order variational equations, we exploit jet transport techniques, which `TaylorIntegration.jl` has fully implemented[9]. The idea of jet transport is the following: given any initial value problem defined by a smooth ordinary differential equation (ODE) $\dot{\mathbf{x}} = \mathbf{f}(t, \mathbf{x})$, together with an initial condition $\mathbf{x}(t_0) = \mathbf{x}_0 \in \mathbb{R}^n$, we propagate a whole neighbourhood $U_{\mathbf{x}_0} \subset \mathbb{R}^n$ of the initial condition $\mathbf{x}_0$. To achieve this, we parameterize $U_{\mathbf{x}_0}$ by expressing an arbitrary point $\mathbf{y} \in U_{\mathbf{x}_0}$ as $\mathbf{y} = \mathbf{x}_0 + \delta\mathbf{x}_0$, where both $\mathbf{x}_0 \in \mathbb{R}^n$ and $\delta\mathbf{x}_0 \in \mathbb{R}^n$. That is, the set of all the allowed values of $\mathbf{x}_0 + \delta\mathbf{x}_0$ represents a parameterization of $U_{\mathbf{x}_0}$. Then, we formally insert the initial condition $\mathbf{x}_0 + \delta\mathbf{x}_0$ into the equations of motion, re-interpreting it as a vector of n multivariate polynomials in the variables $\delta\mathbf{x}_0$. Since the initial condition becomes a polynomial[10], all the computations performed by the numerical integration method have to be done using truncated polynomial algebra, i.e., the algebraic operations (addition, product, etc.) are performed between polynomials and truncating up to a fixed order p. We use the truncated polynomial algebra implemented in `TaylorSeries.jl`[11]. Therefore, by using jet transport, we are able to solve the p-th order variational equation without explicitly programming it in the computer. In this way, with a single numerical integration, we are able to obtain a p-th order polynomial approximation to the propagation of the whole neighbourhood $U_{\mathbf{x}_0}$ up to time t.

Supplementary Note 4: Astrometric treatment

The optical astrometric dataset for Apophis includes 7,902 right-ascension/declination observation pairs from the Minor Planet Center, spanning from March 15th, 2004, through May 12th, 2021. We only exclude 40 observations from January 28th, 2021, performed at the Assy-Turgen Observatory (Minor Planet Center observatory code 217), since they display a systematic bias signature. Our optical astrometry error model accounts for biases present in star catalogs[12], and accounts for other sources of systematic errors via an appropriate weighting scheme[13]. Regarding radar astrometry, we include the 2005–2006 and 2012–2013 datasets, as well as a Doppler shift and three time-delay measurements performed on March 2021 at Goldstone. We use a 7-variable, 5 order jet transport setup, together with a 25-order Taylor expansion with respect to time, which we use to simultaneously estimate the initial conditions and the Yarkovsky effect for Apophis.

We briefly describe the debiasing procedure. Let (α, δ) denote a given optical astrometric observation pair, where α and δ are, respectively, the observed right ascension and declination. Then, for each observation pair (α, δ) we compute the quantities

$$\begin{aligned} \Delta\alpha &= \Delta\alpha_{\mathrm{J2000}} + \Delta\mu_\alpha \cdot \Delta t \\ \Delta\delta &= \Delta\delta_{\mathrm{J2000}} + \Delta\mu_\delta \cdot \Delta t. \end{aligned} \tag{1}$$

Here, $(\Delta\alpha_{\mathrm{J2000}}, \Delta\delta_{\mathrm{J2000}})$ is the correction to the position at the J2000.0 epoch, $\Delta\mu_\alpha$ and $\Delta\mu_\delta$ are the corrections due to proper motion, and Δt is the observation time in years since J2000.0. The computed corrections from Eq. (1) are then subtracted from the observed values for (α, δ). Debiasing tables[12] are provided in terms of the HEALPix tessellation scheme[14], which essentially divides the celestial sphere in equal-area tiles. We compute the transformation from (α, δ) to the corresponding HEALPix tessellation tile index via the `Healpix.jl` package[15].

Supplementary Note 5: Yarkovsky effect estimation from astrometry

In this section, we report two orbital fits to optical and radar astrometry for Apophis which we use to estimate the Yarkovsky effect for Apophis, from the optical and radar astrometry dataset described above, using a 7-DOF Newton method-based orbital fit in a 5th-order, 7-DOF jet transport setup. We proceed by computing two orbital fits: a gravity-only 6-DOF fit (i.e., fixing $A_2 = 0$) to the optical and radar astrometry (solution OR6), and a 7-DOF fit to the optical and radar astrometry including the non-gravitational Yarkovsky acceleration (solution OR7). The initial conditions correspond to the JPL solution #197 at the December 17, 2020 00:00:00.0 (TDB) epoch, which corresponds to the Julian date 2459200.5 (TDB). We present the results for each orbital fit in terms of the position and velocity in Supplementary Table 2, and in Supplementary Table 3 the osculating orbital elements, at the solution epoch referred to J2000.0 heliocentric ecliptic coordinates defined by the IAU 1976 convention[16].

From the Supplementary Tables 2 and 3, we see that, for the OR7 solution (i.e., the 7-DOF fit to the optical and radar astrometry), we obtain $A_2 = (-2.899 \pm 0.025) \times 10^{-14}$ au d^{-2} for the Yarkovsky transverse parameter. This corresponds to a secular semi-major axis drift[17] $(-13.3 \pm 0.1) \times 10^{-4}$ au Myr^{-1}, or (-199.0 ± 1.5) m yr^{-1}. This value is well within the 1-σ formal uncertainty with respect to the estimates obtained previously[7,18–20], which were performed before the close approach of Apophis with Earth during late 2020 and early 2021. Furthermore, our result is consistent with preliminary results which include high-quality optical astrometric observations obtained shortly after Apophis last solar conjunction[21].

We validate the convergence of our orbital fitting procedure by performing the same analysis using 6-th order and 7-th order polynomials in 7 variables, obtaining essentially the same results. Therefore, the loss of accuracy in the fitting due to the truncation of the jet transport solution to a 5-th order polynomial, is negligible. We also validated the integrator using a 30-th order Taylor expansion with a 10^{-30} tolerance, again leaving the results essentially unchanged. Finally, we considered the effect of including 32 most massive main-belt asteroid perturbers instead of 16, as has been done previously[2,19,22], finding no significant modification of the orbital solutions.

Supplementary Note 6: Computation of b-plane coordinates via jet transport

Given an asteroid's close approach to Earth, and a p-th order jet transport integration $\mathbf{x}(t, \delta\mathbf{x}_0)$ describing the asteroid's orbital motion, we compute the time of closest approach t_{CA} as a p-th order polynomial in the variables $\delta\mathbf{x}_0$; i.e., we have $t_{\mathrm{CA}} = t_{\mathrm{CA}}(\delta\mathbf{x}_0)$. From this, for the nominal orbit we compute[23] Öpik's coordinates (ξ, ζ) as a p-th order polynomial in the variables $\delta\mathbf{x}_0$. Next, we differentiate these expressions with respect to $\delta\mathbf{x}_0$ to obtain the Jacobian J of the coordinate transformation from $\mathbf{x}_0$ to (ξ, ζ). Then, using the covariance matrix C associated to the nominal orbit, we compute the covariance matrix C' corresponding to the projection of the orbital uncertainty on the b-plane via a similarity transformation: $C' = J^T \times C \times J$. From C', together with the nominal (ξ, ζ) coordinates, we compute the intersection of a given Valsecchi circle with the uncertainty region, thus producing the ζ value corresponding to a resonant return.

Supplementary Table 1: Value of Gm for the 16 main-belt asteroid perturbers used in our calculations[2].

Body	IAU no.	Gm_i [au^{3}d^{-2}]
Ceres	1	1.400476556172344$\times10^{-13}$
Vesta	4	3.854750187808810$\times10^{-14}$
Pallas	2	3.104448198938713$\times10^{-14}$
Hygiea	10	1.235800787294125$\times10^{-14}$
Euphrosyne	31	6.343280473648602$\times10^{-15}$
Interamnia	704	5.256168678493662$\times10^{-15}$
Davida	511	5.198126979457498$\times10^{-15}$
Eunomia	15	4.678307418350905$\times10^{-15}$
Juno	3	3.617538317147937$\times10^{-15}$
Psyche	16	3.411586826193812$\times10^{-15}$
Cybele	65	3.180659282652541$\times10^{-15}$
Thisbe	88	2.577114127311047$\times10^{-15}$
Doris	48	2.531091726015068$\times10^{-15}$
Europa	52	2.476788101255867$\times10^{-15}$
Patientia	451	2.295559390637462$\times10^{-15}$
Sylvia	87	2.199295173574073$\times10^{-15}$

Supplementary Table 2: International Celestial Reference Frame (ICRF) barycentric initial conditions (position, velocity and nominal Yarkovsky parameter) for the gravity-only (OR6) and non-gravitational (OR7) solutions. The epoch is December 17, 2020 00:00:00.0 (TDB), which corresponds to the Julian date 2459200.5 (TDB). The symbols x_0, y_0, z_0 represent initial positions in au; v_{x0}, v_{y0}, v_{z0} represent initial velocities in au/d. A_2 is the Yarkovsky transverse parameter in au d^{-2}, multiplied by 10^{14}. Numbers in parentheses represent the order of magnitude of the corresponding formal 1-σ uncertainty.

Init. cond./sol.	OR6	OR7
x_0 [au]	$-0.18034816(472) \pm 7.05 \times 10^{-9}$	$-0.18034828(526) \pm 7.12 \times 10^{-9}$
y_0 [au]	$0.94069116(764) \pm 1.71 \times 10^{-9}$	$0.94069105(951) \pm 1.94 \times 10^{-9}$
z_0 [au]	$0.34573641(385) \pm 4.03 \times 10^{-9}$	$0.34573599(029) \pm 5.41 \times 10^{-9}$
v_{x0} [au d^{-1}]	$-0.0162659357(312) \pm 3.31 \times 10^{-11}$	$-0.0162659397(882) \pm 4.79 \times 10^{-11}$
v_{y0} [au d^{-1}]	$4.39163(792) \times 10^{-5} \pm 6.68 \times 10^{-11}$	$4.39154(800) \times 10^{-5} \pm 6.72 \times 10^{-11}$
v_{z0} [au d^{-1}]	$-0.000395210(949) \pm 1.24 \times 10^{-10}$	$-0.000395204(013) \pm 1.38 \times 10^{-10}$
A_2 [$\times 10^{14}$ au d^{-2}]	0.0 (fixed)	$-2.8(988) \pm 2.48 \times 10^{-2}$

Supplementary Table 3: J2000.0 heliocentric IAU1976 ecliptic orbital elements and Yarkovsky transverse parameter for the gravity-only (OR6) and non-gravitational (OR7) solutions. The epoch is December 17, 2020 00:00:00.0 (TDB), which corresponds to the Julian date 2459200.5 (TDB). The orbital elements e, q, t_p, Ω, ω and I represent, respectively, eccentricity, perihelion distance, time of perihelion passage, longitude of ascending node, argument of perihelion and inclination. Numbers in parentheses represent the order of magnitude of the corresponding formal 1-σ uncertainty.

Element/sol.	OR6	OR7
e	$0.19150875(472) \pm 1.28 \times 10^{-9}$	$0.19150886(716) \pm 1.60 \times 10^{-9}$
q [au]	$0.74585316(035) \pm 1.23 \times 10^{-9}$	$0.74585305(033) \pm 1.54 \times 10^{-9}$
t_p [JDTDB]	$2459101.040820(608) \pm 7.49 \times 10^{-7}$	$2459101.04092(537) \pm 1.17 \times 10^{-6}$
Ω [deg]	$204.04254(376) \pm 7.44 \times 10^{-6}$	$204.04199(116) \pm 8.81 \times 10^{-6}$
ω [deg]	$126.65331(533) \pm 7.58 \times 10^{-6}$	$126.65396(094) \pm 9.37 \times 10^{-6}$
I [deg]	$3.336760(462) \pm 1.36 \times 10^{-7}$	$3.336773(201) \pm 1.74 \times 10^{-7}$
A_2 [$\times 10^{14}$ au d^{-2}]	0.0 (fixed)	$-2.8(988) \pm 2.48 \times 10^{-2}$

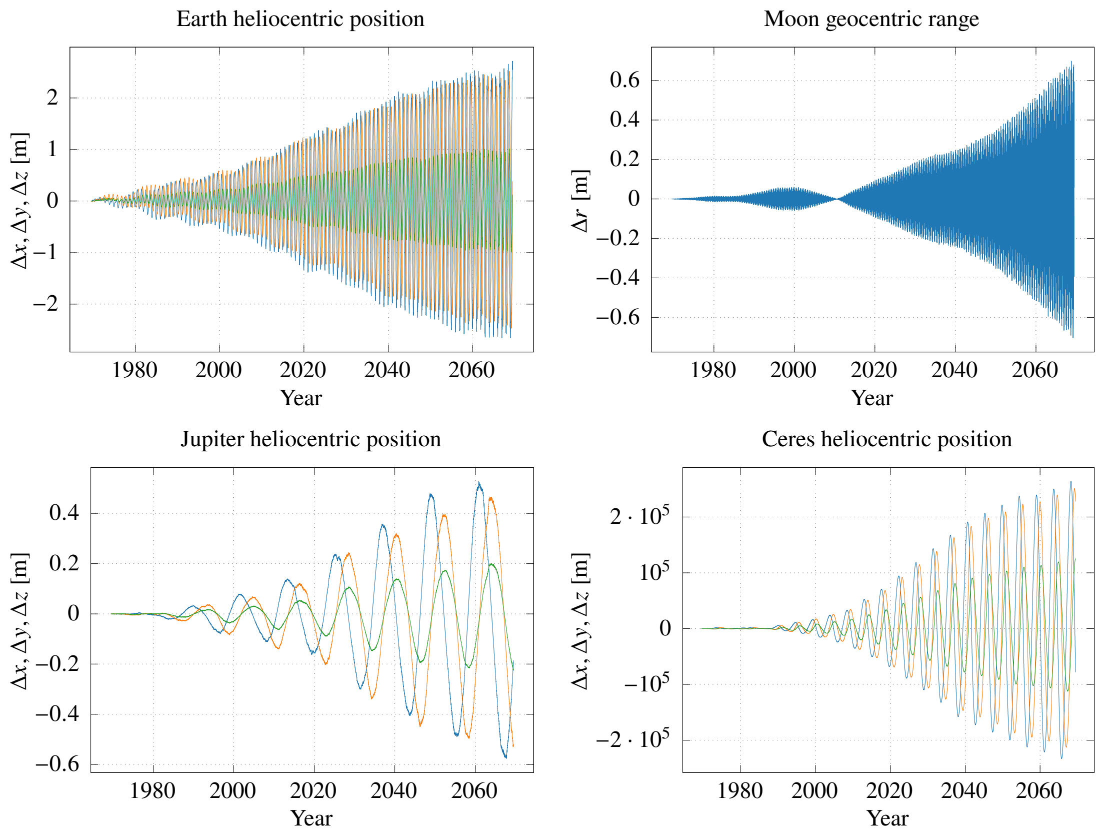

Supplementary Figure 1: **Some comparisons of DE430 and our planetary ephemeris integrations.**

Top left panel: Earth heliocentric absolute position difference. Top right panel: Moon geocentric range absolute difference. Bottom left panel: Jupiter heliocentric absolute position difference. Bottom right panel: Ceres heliocentric absolute position difference. The horizontal axis of all panels represents time.

Supplementary References

1. Pérez-Hernández, J. A. *Dynamics of Near-Earth objects: the Yarkovsky effect for asteroid Apophis and the Lyapunov spectrum of Halley's comet*. Ph.D. thesis, Universidad Nacional Autónoma de México (2021).

2. Folkner, W., Williams, J., Boggs, D., Park, R. & Kuchynka, P. The planetary and lunar ephemerides DE430 and DE431. *Interplanet. Netw. Prog. Rep* **196**, 1–81 (2014).

3. Lieske, J., Lederle, T., Fricke, W. & Morando, B. Expressions for the precession quantities based upon the IAU/1976/system of astronomical constants. *Astronomy and Astrophysics* **58**, 1–16 (1977).

4. Moyer, T. Formulation for observed and computed values of Deep Space Network observables (2003).

5. Standish, E. M. & Williams, J. G. Orbital ephemerides of the Sun, Moon and Planets. In Urban, S. & Seidelmann, P. (eds.) *Explanatory Supplement to the Astronomical Almanac*, chap. 8 (Oxford University Press, 2014).

6. Williams, J. G. & Boggs, D. H. Secular tidal changes in lunar orbit and Earth rotation. *Celestial Mechanics and Dynamical Astronomy* **126**, 89–129 (2016). URL `https://doi.org/10.1007/s10569-016-9702-3`.

7. Brozović, M. *et al.* Goldstone and Arecibo radar observations of (99942) Apophis in 2012–2013. *Icarus* **300**, 115–128 (2018).

8. Jorba, À. & Zou, M. A software package for the numerical integration of ODEs by means of high-order Taylor methods. *Exp. Math.* **14**, 99 (2005). URL `https://doi.org/10.1080/10586458.2005.10128904`.

9. Pérez-Hernández, J. A. & Benet, L. TaylorIntegration.jl v0.8.3: ODE integration using Taylor's method in Julia (2021). URL `https://github.com/PerezHz/TaylorIntegration.jl`.

10. Pérez-Palau, D., Masdemont, J. & Gómez, G. Tools to detect structures in dynamical systems using jet transport. *Celestial Mechanics and Dynamical Astronomy* **123**, 239–262 (2015). URL `https://doi.org/10.1007/s10569-015-9634-3`.

11. Benet, L. & Sanders, D. P. TaylorSeries. jl: Taylor expansions in one and several variables in Julia. *Journal of Open Source Software* **4**, 1043 (2019).

12. Eggl, S., Farnocchia, D., Chamberlin, A. B. & Chesley, S. R. Star catalog position and proper motion corrections in asteroid astrometry II: The Gaia era. *Icarus* **339**, 113596 (2020).

13. Vereš, P., Farnocchia, D., Chesley, S. R. & Chamberlin, A. B. Statistical analysis of astrometric errors for the most productive asteroid surveys. *Icarus* **296**, 139–149 (2017).

14. Gorski, K. M. *et al.* Healpix: A framework for high-resolution discretization and fast analysis of data distributed on the sphere. *The Astrophysical Journal* **622**, 759 (2005).

15. Tomasi, M. & Li, Z. Healpix.jl: Julia-only port of the HEALPix library (2021). `2109.028`.

16. Lederle, T. The IAU (1976) System of Astronomical Constants. *Mitteilungen der Astronomischen Gesellschaft Hamburg* **48**, 59–65 (1980).

17. Farnocchia, D. *et al.* Near Earth asteroids with measurable Yarkovsky effect. *Icarus* **224**, 1–13 (2013). URL https://doi.org/10.1016/j.icarus.2013.02.004.

18. Vokrouhlický, D. *et al.* The Yarkovsky effect for 99942 Apophis. *Icarus* **252**, 277–283 (2015). URL https://doi.org/10.1016/j.icarus.2015.01.011.

19. Del Vigna, A. *et al.* Detecting the Yarkovsky effect among near-Earth asteroids from astrometric data. *Astronomy & Astrophysics* **617**, A61 (2018). URL https://doi.org/10.1051/0004-6361/201833153.

20. Greenberg, A. H., Margot, J.-L., Verma, A. K., Taylor, P. A. & Hodge, S. E. Yarkovsky drift detections for 247 near-Earth asteroids. *The Astronomical Journal* **159**, 92 (2020).

21. Tholen, D. & Farnocchia, D. Detection of yarkovsky acceleration of (99942) apophis. In *AAS/Division for Planetary Sciences Meeting Abstracts*, vol. 52, 214–06 (2020). URL https://baas.aas.org/pub/2020n6i214p06.

22. Farnocchia, D. *et al.* Yarkovsky-driven impact risk analysis for asteroid (99942) Apophis. *Icarus* **224**, 192–200 (2013). URL https://doi.org/10.1016/j.icarus.2013.02.020.

23. Farnocchia, D., Eggl, S., Chodas, P. W., Giorgini, J. D. & Chesley, S. R. Planetary encounter analysis on the B-plane: a comprehensive formulation. *Celestial Mechanics and Dynamical Astronomy* **131**, 36 (2019).